Supplemental Material for "Asymmetry in energy versus spin transport in certain interacting, disordered systems"

SIMULATION OF TWO-SITE DRIVING SCHEME

In the following we describe how the two-site driving protocol for inducing a nonequilibrium NESS in a disordered lattice is implemented, and present details of its numerical simulation.

Defining target states for energy and spin driving

To study spin and energy transport across disordered spin lattices, we simulate the nonequilibrium configuration depicted in Fig. 1(a). Here the two left-most (L) and right-most (R) sites are coupled to reservoirs of different temperature and chemical potential. Let β_k and μ_k be the target inverse temperature and chemical potential characterizing the target state ρ_k that reservoir k tries to impose at the k boundary (k = L,R). The corresponding grand-canonical state for $m > 2$ sites is

$$\begin{aligned} \rho_k^{(m)} &= \exp\left(\beta_k\left(-H_k^{(m)} + \mu_k M^{(m)}\right)\right)/Z_k^{(m)}, \\ Z_k^{(m)} &= \mathrm{Tr}\left[\exp\left(\beta_k\left(-H_k^{(m)} + \mu_k M^{(m)}\right)\right)\right], \end{aligned} \tag{S1}$$

where $H_k^{(m)}$ is the Hamiltonian for the m sites at boundary k, $M^{(m)} = \sum_{i=1}^{m} s_i^z$ is the magnetization operator for the m sites, and $Z_k^{(m)}$ is the corresponding partition function. The two-site target state ρ_k results from tracing out the $m-2$ most internal sites from $\rho_k^{(m)}$. Once the target states are defined for both left and right boundaries for a particular value of m (we take $m = 4$), the Lindblad dissipators $\mathcal{L}_k$ are built so that $\mathcal{L}_k(\rho_k) = 0$, with the coupling strength between the chain and the reservoirs being $\Gamma = 1$. Full details of how this is done are given in several references [1–4], which we summarize below. We emphasize that even though a microscopic derivation of master equation (2) with the described two-site driving might be quite challenging [5], the transport properties we obtain in the bulk are independent of the details of such driving for the system sizes we take in our calculations [6]. Thus we also note that these bulk transport properties are not affected by taking $H_k^{(m)}$ as the m-site Hamiltonian of the clean model, which we do for the finite magnetization simulations.

Several nonequilibrium configurations can be induced by choosing different values of β_k and μ_k. In our work we are interested in two cases. Firstly we consider energy transport for zero total magnetization, where $\beta_\mathrm{L} < \beta_\mathrm{R}$ and $\mu_\mathrm{L} = \mu_\mathrm{R} = 0$. In particular, our simulations were performed with $\beta_\mathrm{L} = 4 \times 10^{-3}$ and $\beta_\mathrm{R} = 4 \times 10^{-2}$. This leads to a NESS in which an energy flow is established from left to right, with negligible net magnetization flow across the lattice. Secondly we discuss the case of a temperature imbalance beyond half filling, where $\beta_\mathrm{L} < \beta_\mathrm{R}$ and $\beta_\mathrm{L}\mu_\mathrm{L} = \beta_\mathrm{R}\mu_\mathrm{R} > 0$. Specifically, for our simulations we took the same temperature imbalance and $\beta_k\mu_k = 1$. Here a significant spin current emerges in addition to the energy flow, which features a different nature to the spin transport at zero magnetization and no temperature imbalance [6], as discussed in the main text.

Building the driving superoperator

Now we briefly describe how to create a two-site bath superoperator $\mathcal{L}$ inducing a target state ρ as the NESS of a pair of isolated sites, such that

$$\mathcal{L}(\rho) = 0. \tag{S2}$$

We need to define $\mathcal{L}$ so that ρ is its only eigenvector with zero eigenvalue, and that all the other eigenvalues are equal to -1. This leads to the fastest possible convergence to ρ [1]. For this, we first diagonalize the target state, $\rho = V^\dagger d V$, and obtain the "diagonal" superoperator $\mathcal{L}^\mathrm{diag}$ for which the diagonal matrix d is the only zero-eigenvalue eigenstate,

$$\mathcal{L}^\mathrm{diag}(d) = 0. \tag{S3}$$

The matrix elements of the "diagonal" superoperator are determined depending on the particular definition of the two-site operator-space basis Ω_n ($n = 0, \ldots, 15$). For example, for $\Omega_n = (\sigma_{n_1} \otimes \sigma_{n_2})/4$, with σ_{n_α} ($\alpha = 1, 2$) the Pauli matrices plus the identity ($n_\alpha = 0, \ldots, 3$), the exact form of $\mathcal{L}^\mathrm{diag}$ is given in Refs. [1, 4] for two different orders of the Pauli basis.

Once $\mathcal{L}^\mathrm{diag}$ is built, the total superoperator $\mathcal{L}$ is obtained through a rotation in operator space,

$$\mathcal{L} = R^\dagger \mathcal{L}^\mathrm{diag} R. \tag{S4}$$

The elements of the rotation matrix R are given by

$$R_{i,j} = \frac{1}{4}\mathrm{tr}(V^\dagger \Omega_i V \Omega_j), \tag{S5}$$

thus being defined through V.

Details on numerical simulation method

To obtain the NESS of the system for each set of parameters, we consider M realizations of the disordered magnetic field. For each realization r we simulate the

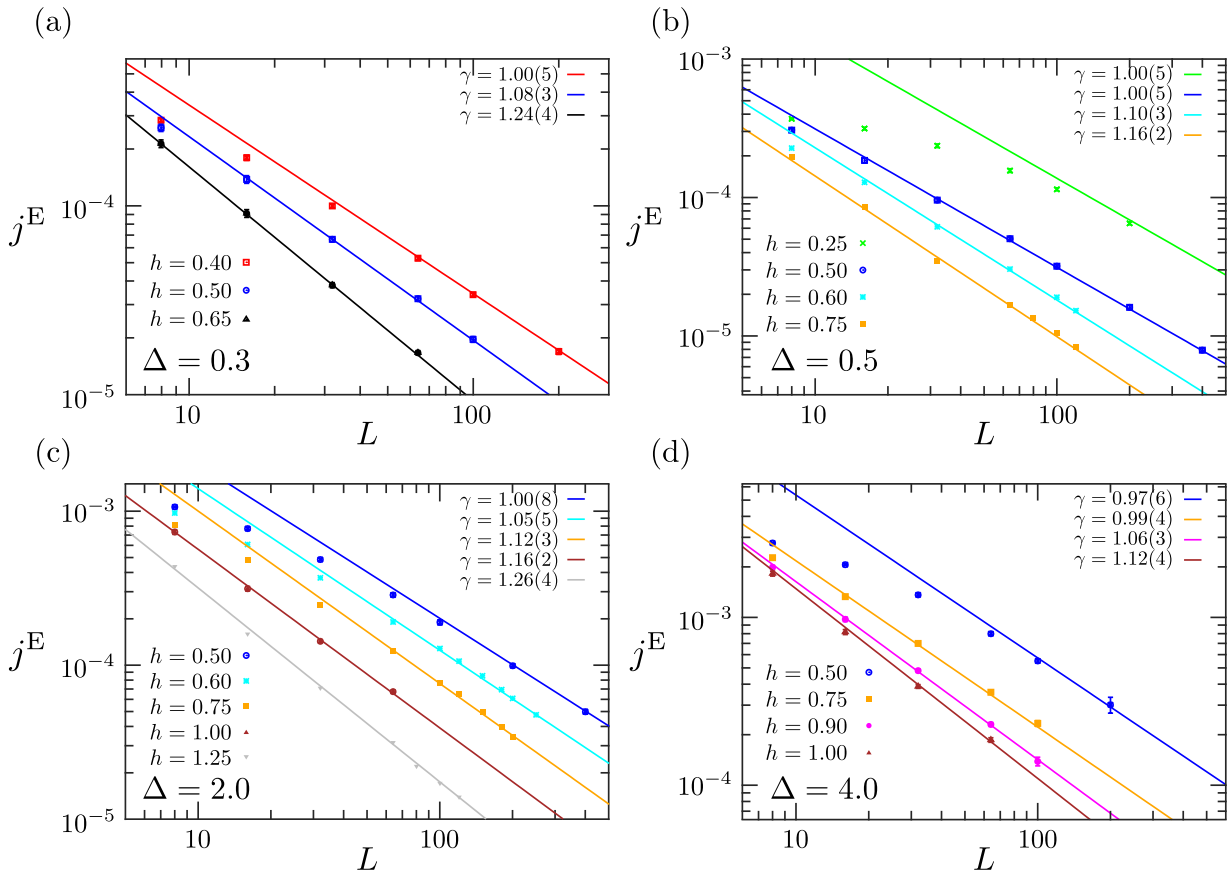

FIG. S1: Transport at zero magnetization, showing scaling of energy current in NESS for various anisotropies Δ and disorder strengths h. As in Fig. 2(b) of the main text, the disorder strength h increases from top to bottom in each plot. We find that stronger disorders are required for the onset of subdiffusion as we enter the Ising regime.

long-time evolution of the density matrix of the lattice, given by $\rho_\infty^{(r)} = \lim_{t\to\infty} \exp(\mathcal{L}^{(r)}t)\rho(0)$, with $\rho(0)$ the initial state. A unique NESS $\rho_\infty^{(r)}$ is obtained after evolving for a long-enough time from any $\rho(0)$, guaranteed due to the ergodicity of the bulk coherent dynamics [1]. We take $\rho(0)$ as a product state with homogeneous magnetization $\langle s_i^z\rangle = \beta_k\mu_k/4$, which is the value imposed by the driving on two isolated sites.

The time-evolution simulation is performed using the t-DMRG technique, which allows us to analyze spin chains of hundreds of lattice sites. The algorithm is based on a Suzuki-Trotter decomposition [7] of the Lindblad evolution operator. Here at any time t the density matrix of the system $\rho^{(r)}(t)$ is described by a matrix product operator (MPO) with matrix dimension of up to $\chi = 150$, and its time evolution is calculated by a sequence of two-site gates corresponding to applications of local evolution operators [8]. This process is performed until the currents become homogeneous across the lattice, which indicates that the NESS has been reached.

After the NESS is obtained for M realizations (taking up to $M = 200$ for small system sizes), the expectation values of interest are averaged over all of them, getting maximal statistical uncertainty of $\sigma(j^E)/\sqrt{M} \approx 2\%$ for the zero-magnetization sector and of $\approx 3-4\%$ for the harder-to-simulate nonzero magnetization transport, with $\sigma(j^E)$ the standard deviation of the NESS energy current when averaged over all the disorder realizations and across the lattice.

ADDITIONAL CURRENT SCALING

In Fig. 2(b) of the main text, we showed that from the current scalings for different anisotropies Δ we may claim that (i) there is a transition from diffusive to subdiffusive transport of energy as a function of disorder strength; (ii) this critical disorder strength is far from the localization transition. Similar conclusions also hold for other weaker and stronger anisotropies as shown in Fig. S1. However we note that as we increase the Ising anisotropy, the diffusive regime also increases i.e. a larger portion of the Hamiltonian-paramater space is diffusive before the onset of subdiffusion. Thus we have a regime where spin is transported subdiffusively whereas the energy is transported diffusively; a particular instance is shown in Fig.

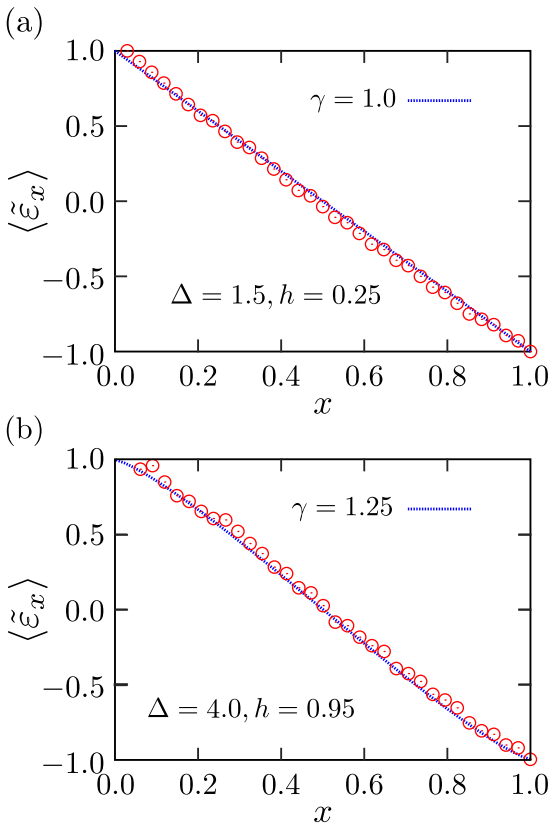

FIG. S2: Rescaled energy profiles averaged over disorder for $L = 64$ and parameters leading to different type of energy transport (symbols), and fits using a spatially varying diffusion constant $D(x) \propto [x(1-x)]^{1-\gamma}$ for *bulk* transport (dotted lines); 20-30% of either ends of the chain has been removed. (a) Naive NESS current scaling would give superdiffusive behaviour from finite-L, which from the profile nicely shows diffusion instead. (b) Here at large anisotropy and disorder the bulk still shows nice subdiffusive scaling despite 50% of the edges being removed.

3 where this phenomenon is seen more clearly.

Collecting all data from Fig. 2 and Fig. S1 results in the dynamical phase diagram Fig. 1(b).

ENERGY PROFILES AND BULK TRANSPORT

A point to note from Fig. 2 and Fig. S1 is that for very weak disorder fields $h = 0.25$, the thermodynamic limit is reached only very slowly and fitting a straight line is problematic. Nevertheless we have drawn a $1/L$ diffusive fit that looks like it will asymptotically be parallel to the data. To better characterize the transport in this and similar cases, we defined rescaled and shifted energy profiles $\langle \tilde{\varepsilon}_x \rangle$ so $-1 \leq \langle \tilde{\varepsilon}_x \rangle \leq 1$, and fitted them to generalized diffusion equations with spatially dependent diffusion constants [6], as shown in Fig. S2. Here the slowest asymptoting (most nondiffusive i.e. naively superdiffusive fit with $\gamma = 0.9$) case of $h = 0.25$, $\Delta = 1.5$ clearly shows diffusive scaling in the bulk (Fig. S2(a)). A $\gamma < 1$ fit to the energy profile cannot be reasonably made, thereby discounting superdiffusive transport for bulk physics. For $h = 0.95$, $\Delta = 4$ (Fig. S2(b)) where the data already converged (Fig. S1) to subdiffusive transport, the energy profile provides a quantitatively consistent result (albeit a slightly different numerical value for the exponent).

SHORT TIME EXPANSION

A short time expansion of current-current correlators is possible in order to glean some transport properties of the two conserved quantities of the model [9]. These are fully characterized by the moments μ_k, $k > 0$,

$$\langle j(t)j(0)\rangle \equiv \sum_{k=0}^{\infty} \frac{\mu_k}{(2k)!} t^{2k}, \tag{S6}$$

where $j = \sum_i j_i$ is the total current in the system, and $j(t)$ is its Heisenberg representation.

At high-temperature and for uncorrelated disorder with variance $\frac{h^2}{3}$ (so that off-site terms such as $h_i h_j$, with $i \neq j$, average out to zero) we find may compute the moments to be

$$\begin{aligned}
\langle j^S(t)j^S(0)\rangle &= \frac{J^2}{8} + \frac{J^2}{16}\left(\Delta^2 + \frac{4h^2}{3}\right)t^2 + \frac{J^2}{64}\left[\Delta^2(4\Delta^2+5J^2) + h^2(4J^2+16\Delta^2) + \frac{128h^4}{15}\right]t^4 + \ldots, \\
\langle j^E(t)j^E(0)\rangle &= \frac{J^2}{96}\left(3J^2+6\Delta^2+4h^2\right) + \frac{J^2h^2}{720}\left[45J^2+28h^2+45\Delta^2\right]t^2 + \ldots
\end{aligned} \tag{S7}$$

We note the following checks before proceeding with the analysis:

1. For $\Delta = h = 0$ both have only a nondecaying Drude weight component (i.e. long-time plateau in the correlator $\lim_{t\to\infty}\langle j(t)j(0)\rangle$), as expected for tight-binding model.

2. For $h = 0$ the time dependence in the second line of Eq. (S7) drops out, as expected for energy transport in the XXZ model, but does not in the first one, as expected for spin conduction.

3. For $\Delta = 0$ both have a time-dependence with a different sum-rule governed by $\mu_0 = \int_{-\infty}^{+\infty}\sigma(\omega)\frac{d\omega}{2\pi}$, as expected for a noninteracting spin-chain.

Similarly for the integrability broken chain with next-nearest neighbour interactions Δ_2, we find the following expansions:

$$\begin{aligned}
\langle j^S(t)j^S(0)\rangle &= \frac{J^2}{8} + \frac{J^2}{16}\left(\Delta^2 - 2\Delta\Delta_2 + 2\Delta_2^2\right)t^2 \\
&+ \frac{J^2}{64}\left[J^2(5\Delta^2 - 16\Delta\Delta_2 + 17\Delta_2^2) + 4(\Delta^4 - 4\Delta^3\Delta_2 + 9\Delta^2\Delta_2^2 - 10\Delta\Delta_2^3 + 5\Delta_2^4)\right]t^4 + \ldots, \\
\langle j^E(t)j^E(0)\rangle &= \frac{J^2}{32}\left(J^2 + 2\Delta^2 - 2\Delta\Delta_2 + 6\Delta_2^2\right) + \frac{J^2\Delta_2^2}{64}\left[17J^2 + 8\Delta^2 - 16\Delta\Delta_2 + 10\Delta_2^2\right]t^2 + \\
&+ \frac{J^2\Delta_2^2}{256}\left[444J^4 + 24\Delta^4 - 112\Delta^3\Delta_2 + 416J^2\Delta_2^2 + 88\Delta_2^4 - 27\Delta\Delta_2(17J^2 + 8\Delta_2^2) + 2\Delta^2(89J^2 + 112\Delta_2^2)\right]t^4 \\
&\ldots
\end{aligned} \tag{S8}$$

From Eqs. (S7) and (S8) and assuming we are perturbing, with weak disorder h or Δ_2, the initial (broadened) delta function conductivity (valid for all Δ for energy but only at low Δ for spin) and given by

$$\sigma(\omega) = \mathcal{F}\left\{\langle j(t)j\rangle\right\}, \tag{S9}$$

where $\mathcal{F}$ denotes the real-Fourier transform, is approximated by:

$$\sigma(\omega) = \frac{\mathcal{A}}{\sqrt{\pi}\omega_0}\mathrm{e}^{-(\frac{\omega}{\omega_0})^2}. \tag{S10}$$

The above two unknowns $\mathcal{A}, \omega_0$ are computed by matching against the moments μ_n so that the conditions $\mu_n = \int_{-\infty}^{+\infty}\omega^{2n}\sigma(\omega)\frac{d\omega}{2\pi}$ are satisfied for $n = 0, 1$. Taking density of states to be $\mathcal{O}(1)$ at infinite temperature, this approximates the diffusion constant $\mathcal{D} \propto \sigma(\omega \to 0)$ by $\mathcal{D} = \sqrt{\frac{\mu_0^3}{\mu_1}}$. This implies, for the two quantities:

$$\begin{aligned}
\mathcal{D}_S(h) &\sim \frac{J^2}{\sqrt{6\Delta^2 + 8h^2}}, \\
\mathcal{D}_E(h) &\sim \frac{\kappa^2}{h},
\end{aligned} \tag{S11}$$

where

$$\kappa = \left\{ \begin{array}{l} J^2, \text{ if } \Delta \ll 1 \\ \Delta J, \text{ if } \Delta \gg 1 \end{array} \right\}$$

A qualitatively similar dependence is also seen for the next-nearest-neighbour interacting case, with different coefficients $\mathcal{O}(1)$, as may be seen by taking the ratios $\sqrt{\frac{\mu_0^3}{\mu_1}}$ for spin and energy using Eq. (S8). The main point to highlight from this result is that the divergence with h of the diffusion constants is different for energy and spin. Note however that the precise forms of divergences do not fully reproduce known results. In particular (a) $\mathcal{D}_S$ does not even really diverge with h unless $\Delta = 0$, whereas it should do so with a power between 0.66 and 2 [6] for $\Delta \leq 1$. (b) Only very few moments are employed, so genuine low-frequency physics is missed.

However the above argument does show a stronger divergence for the energy-energy autocorrelation at small h. For example, fixing $h \ll 1$ and $\Delta \gg 1$ in Eq. (S7) indeed gives a much larger diffusion constant for energy than for spin transport, which we might interpret as supportive of the diffusion vs. subdiffusion scenario and thus are in the same qualitative direction of our numerics.

We have used the DiracQ package [10] for automating the short-time expansions.

[1] T. Prosen and M. Žnidarič, J. Stat. Mech. p. P02035 (2009).
[2] M. Žnidarič, T. Prosen, G. Benenti, G. Casati, and D. Rossini, Phys. Rev. E **81**, 051135 (2010).
[3] M. Žnidarič, J. Stat. Mech. **2011**, P12008 (2011).
[4] J. J. Mendoza-Arenas, S. R. Clark, and D. Jaksch, Phys. Rev. E **91**, 042129 (2015).
[5] H.-P. Breuer and F. Petruccione, *The theory of open quantum systems* (Oxford University Press, Oxford, 2002).

[6] M. Žnidarič, A. Scardicchio, and V. Varma, Phys. Rev. Lett. **117**, 040601 (2016).
[7] M. Suzuki, Phys. Lett. A **146**, 319 (1990).
[8] M. Žnidarič, J. J. Mendoza-Arenas, S. R. Clark, and J. Goold, Annalen der Physik **529**, 1600298 (2017).
[9] R. J. Sánchez, V. K. Varma, and V. Oganesyan, Phys. Rev. B **98**, 054415 (2018).
[10] J. Wright and B. S. Shastry, *DiracQ: A Quantum Many-Body Physics Package* (arXiv:1301.4494 [cond-mat,str-el], 2013).